Rheol Acta
DOI 10.1007/s00397-008-0276-1

ORIGINAL CONTRIBUTION

Lubricated compression of BMC, a concentrated and fibre-reinforced granular polymer suspension

Laurent Orgéas · Pierre J. J. Dumont · Thai-Hung Le · Denis Favier

Received: 16 February 2008 / Accepted: 23 February 2008

Abstract Bulk moulding compounds (BMCs) are thermoset polymer composites widely used in electric and automotive industries. During their processing by injection, BMCs look like fibre-reinforced granular suspensions in the form of pastes, the rheology of which is not well known. For that purpose, lubricated compression tests were performed on BMC samples with various formulations. Firstly, results show that samples flow without sticking to the rheometer's plates, validating the efficiency of the lubricant. A correction, which requires few assumptions on the rheology of BMC, is then proposed to account for its contribution to the overall axial stress. Thereby, the influences of the axial strain rate, the loading path, the polydispersity of the mineral filler and the fibre content on the BMC flow are analysed. A 1D elementary non-linear viscoelastic model is proposed to capture the main observed trends.

Keywords BMC · Polymer composites · Fibre-reinforced granular suspension · Compression rheometer

Paper presented at 4th Annual European Rheology Conference, April 12–14, 2007, Naples, Italy.

L. Orgéas (✉) · T.-H. Le · D. Favier
Laboratoire Sols-Solides-Structures-Risques (3SR), CNRS - Université de Grenoble (INPG-UJF), BP 53, 38041 Grenoble cedex 9, France
e-mail: Laurent.Orgeas@hmg.inpg.fr

P. J. J. Dumont
Laboratoire de Génie des Procédés Papetiers (LGP2), CNRS-INPG-EFPG, BP 65, 461, rue de la Papeterie, 38402 Saint-Martin-d'Hères, France

Introduction

Bulk moulding compounds (BMCs) are composite materials that are made up of a pasty filled thermoset polymer matrix reinforced by entangled short glass fibres. They offer high corrosion resistance and make it possible to design parts integrating several functionalities in a large spectrum of shapes at low cost. They are widely used by the electric industry to produce small components having good surface appearance and complex shapes. Their processing route can be split into three main phases: (1) the compounding phase, which consists in mixing altogether the uncured polyester, the mineral fillers, glass-fibre bundles and other additives; (2) the injection moulding phase (1–10 s) inside a hot mould ($\approx 150^\circ$ C) and (3) the polymer curing within the hot mould (60–180 s).

Studies devoted to the chemo-rheological behaviour of BMCs during their processing are scarce. They mainly concern the curing stage by focusing on the influence of the type of granular and fibrous fillers and other additives (Kenny and Opalicki 1996; Ma et al. 2003), the influence of the temperature and confining pressure (Millischer and Delaunay 2001) and the polyester shrinkage (Deslandes et al. 1998; Vallat et al. 1999; Vayer et al. 2002; Ma et al. 2003; Boyard et al. 2007). By contrast, the rheology of BMCs during the injection moulding phase has been less studied. By studying flow mechanisms occurring during the injection inside a transparent mould, Lafranche et al. (2002) have shown that the BMC flow inside the mould associates shear and elongational deformation modes. Two other pioneering studies focused more precisely on the BMC rheology and concluded with a temperature-dependent shear-thinning behaviour (Blanc et al. 1992;

Kenny and Opalicki 1996). However, BMCs were subjected to heterogenous deformation modes. Under such circumstances, it is very difficult to study their rheology without a priori constitutive assumptions. Moreover, characteristic dimensions of flowing zones in the used rheometers were not large enough compared with the typical length of glass fibres contained in BMC. This may increase the variability of experimental results and hide some experimental trends (Dumont et al. 2003).

Hence, no data concerning the BMC rheology using large samples subjected to homogeneous loading cases can be found in the literature. This would allow a better analysis of the rheology of these materials without a priori constitutive assumptions and reduced scattering.

For that purpose, various BMC formulations with three fibre contents and two mineral fillers displaying different particle size distributions were collected at the outlet of an industrial injection machine ("Materials" section). Large cylindrical BMC samples were produced, their top and bottom surfaces being carefully lubricated. They were then deformed under simple compression deformation mode at constant axial strain rates ("Experimental procedure" section). Compression data were corrected to account for the influence of the lubrication layers put between the samples and the rheometer plates ("Analysis of compression tests" section). Experimental results emphasize the influence of the imposed strain rate and strain, strain rate loading path, fibre content and mineral fillers' polydispersity on the BMC rheology ("Results" section). Results are then discussed and a simple 1D non-linear viscoelastic model is proposed to reproduce the observed trends ("Discussion" section).

Materials

Studied BMC materials were compounded by Compositec (Le Bourget du Lac, France). The polymer matrix (or paste) forming these materials was prepared using a pneumatic turbine and is composed of 35.25 wt.% of orthophtalic polyester, 2.65 wt.% zinc stearate, 8.8 wt.% moulding agents and 53.30 wt.% of Al_2O_3 fillers. The shear viscosity of the orthophtalic polyester at room temperature was determined using a cone-plate rheometer (Anton Paar, Physica MCR 301). It exhibits a Newtonian shear viscosity of 10 Pa s for shear strain rates ranging from 0.01 to 2500 s^{-1}. Two different size distributions, respectively noted C_1 and C_2, of particles were used. They were measured with a particle sizer (Malvern, Master Sizer X). As shown from the graphs plotted in Fig. 1, both size distributions have a mean particle diameter of ≈ 12 μm, but C_1 is wider than C_2. Final compounds were also prepared by adding to the pasty matrix glass fibre bundles made of approximately 200 fibres of length 6 mm and diameter 13.7 μm. Three mass fractions of glass fibre bundles f were tested, i.e. 0, 10 and 20 wt.%. To account for the influence of the injection screw and convergent on microstructural properties of BMC, the as-compounded materials were poured into an injection screw press (1,000 kN, Compositec) and collected in bags at its exhaust. At this stage, it could be easily seen that fibre bundles were completely disaggregated and that the remaining fibres had been cut, forming a complex intricate network. To analyse quantitatively the fibre length distribution, the collected materials were first charred, to eliminate the polymer from them. Then, mineral fillers were etched with acid and filtered to isolate fibres. Therefrom, the lengths of 5,000 fibres were measured in a specially designed apparatus, initially developed to measure fibre dimensions in paper pulps (TechPap, Morfi LB-01). Results have been gathered in the graph plotted in Fig. 2, which shows the fibre length distribution within the studied BMC. As evident from this graph, fibres have been severely broken: most of them have very short lengths below 0.6 mm.

Experimental procedure

Mechanical tests were performed using a rheometer that allows to deform samples which have characteristic dimensions that are sufficiently large compared to the lengths of fibres. It was especially developed to study the rheology of similar polymer composites, such as Sheet Moulding Compounds (SMC) or Glass Mat Thermoplastics (GMT) (Le Corre et al. 2002; Dumont et al. 2003, 2007b). It was mounted on a MTS mechanical universal tensile testing machine having a maximum capacity of 20 kN and a maximum cross-head velocity of 8 mm s^{-1}.

Cylindrical BMC samples having an initial height h_0 of 25 mm and initial diameters $2R_0$ of 70 or 110 mm (for the BMCs with fibres) or 155 or 250 mm (for the BMCs without fibres) were first processed:

- The initial height h_0 of samples was chosen accounting for the two following constraints: Firstly, it had to be high enough compared to the length of fibres so that a good scale separation would be obtained between the sample height and the local material heterogeneity. Secondly, the height had to be small enough to limit creep of samples at rest before testing.

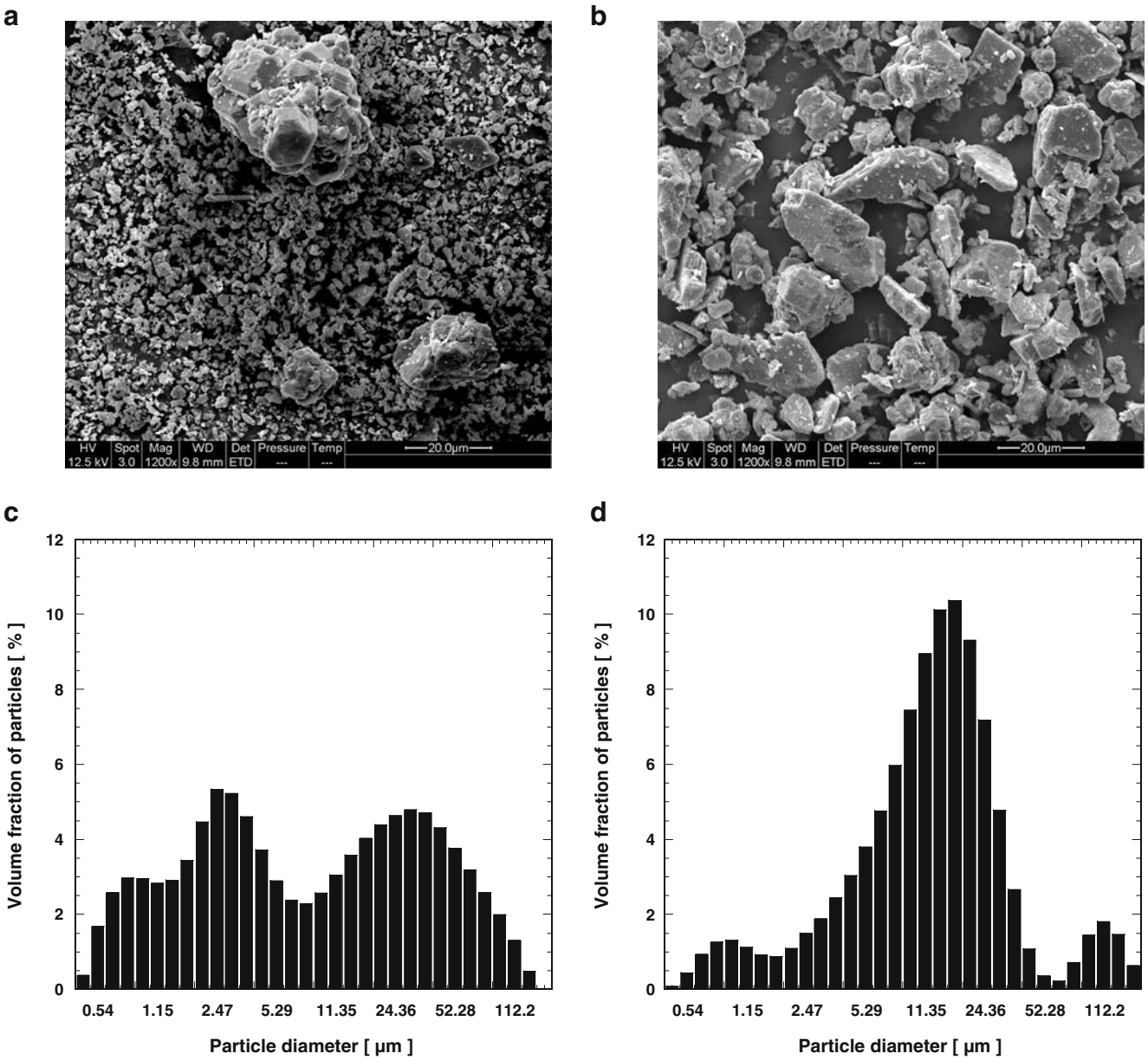

Fig. 1 SEM micrographs (**a**, **b**) and distributions of the particle diameters (**c**, **d**) for the C_1 (**a**, **c**) and the C_2 (**b**, **d**) Al_2O_3 mineral fillers

– The processing route used to produce samples is described as follows: Firstly, a prescribed amount of BMC was extracted from bags and hand-mixed to (1) induce fibrous microstructures with random fibre orientation and (2) pre-shape cylindrical samples close to their final dimensions. Secondly, pre-shaped samples were then put into cylindrical moulds and compressed at a closing force of 20 kN to adjust the final sample dimensions. During this nearly oedometric compaction, flow of BMCs was limited so that microstructures were likely to evolve slightly.

– Special attention was paid to repeat carefully the same processing route for all samples, which allows us to assume that all tested samples have nearly the same initial fibrous microstructures. According to the above methodology, fibrous microstructures should exhibit transverse isotropy, the symmetry axis of which is parallel to the symmetry axis of samples. However, such microstructures have not been characterised in this work: due to the nature of BMCs, this would require very heavy measurements (Le et al. 2008) that one cannot achieve for a large amount of samples, at least for the moment.

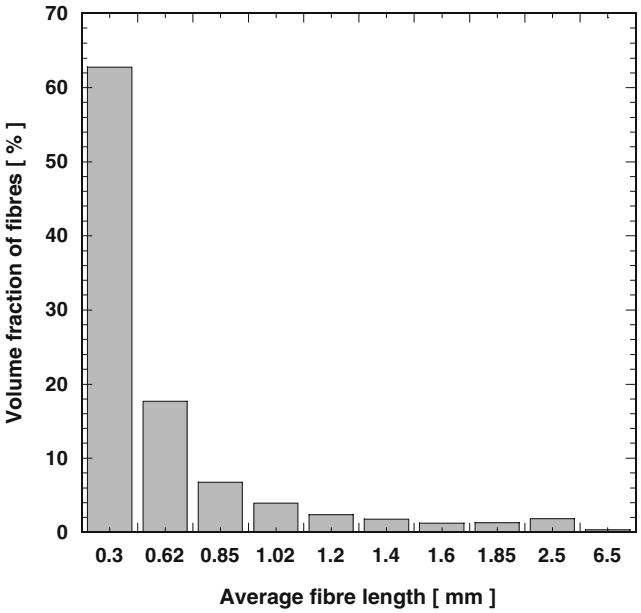

Fig. 2 Distributions of the fibre length at the exhaust of the injection press

Therefrom, samples were compressed in the rheometer at room temperature ($T = 23°C$) and at constant axial strain rates $D_{33} = \dot{h}/h$ along the $\underline{\mathbf{e}}_3$ direction ranging from 10^{-3} to 10^{-1} s^{-1} ($\underline{\mathbf{e}}_3$ is the unit vector associated with the axis of the machine and of the sample and h is the current height of samples).

To impose, a homogeneous simple compression kinematics, i.e. to limit sticking and friction between the mould and the surfaces of samples, the upper and lower surfaces of samples were initially coated with thin silicone grease layers. During the experiments, evolutions of the axial force F_3 and of the current height h of samples were recorded. This allows to estimate the axial logarithmic strain $\varepsilon_{33} = \ln(h/h_0)$ and the mean axial Cauchy stress[1] $\bar{\sigma}_{33} = F_3 h/\pi R_0^2 h_0$ (assuming the incompressibility of BMCs).

Analysis of compression tests

General aspect of compression curves

Figure 3 represents typical evolutions of the mean axial stress $\bar{\sigma}_{33}$ with respect to the axial logarithmic strain ε_{33}. Reported curves have been obtained with five tests performed using the same testing conditions, i.e., a constant axial strain rate $D_{33} = 10^{-1}$ s^{-1}, $f = 20\%$ and with the C_1 formulation. Whatever the considered curve, three stages can be observed during these compressions: in a first step, stress levels increase sharply up to a first inflexion, from which they increase steadily and finally rise sharply when a second inflexion is attained for large strains. It is worth noting that, for axial strains ε_{33} below 1.2, the scattering of the measurements is rather weak and remains below $\pm 10\%$. Also notice that each stress–strain curve that will be plotted in the following will represent an average curve obtained from five runs performed with the same testing conditions, as in the examples shown in Fig. 3.

Flow kinematics

A sixth test was performed using similar testing conditions. However, at various imposed axial strains ε_{33}, i.e. 0.35, 0.7 and 1.2, the test was interrupted and photographs of the deformed sample were taken before the test to restart towards a higher axial strain. Resulting pictures have also been reported in Fig. 3. Firstly, this figure shows that marks previously plotted on the sample deform with it: BMC slips along the plate of the rheometer with no observable sticking zones (Estellé et al. 2006). Also notice that visual observations performed during the test showed that the lateral free surfaces of the sample exhibited rather flat shapes. Secondly, Fig. 3 also shows that it is fair to conclude that the planar deformation of the sample is rather homogeneous (at least at the macroscale) even at very high strains. Consequently, in the following, it will be assumed that the deformation of samples proceeds with homogeneous stress $\underline{\underline{\boldsymbol{\sigma}}}$, strain $\underline{\underline{\boldsymbol{\varepsilon}}}$ and strain rate $\underline{\underline{\mathbf{D}}}$ states corresponding to a simple compression loading. By assuming that BMC samples are incompressible and may display transverse isotropy of axis $\underline{\mathbf{e}}_3$, this yields in the cylindrical coordinates basis $(\underline{\mathbf{e}}_r, \underline{\mathbf{e}}_\theta, \underline{\mathbf{e}}_3)$:

$$\underline{\underline{\boldsymbol{\sigma}}} = \sigma_{33}\underline{\mathbf{e}}_3 \otimes \underline{\mathbf{e}}_3, \tag{1}$$

$$\underline{\underline{\boldsymbol{\varepsilon}}} = \varepsilon_{33}\left(\underline{\mathbf{e}}_3 \otimes \underline{\mathbf{e}}_3 - \frac{1}{2}\underline{\mathbf{e}}_r \otimes \underline{\mathbf{e}}_r - \frac{1}{2}\underline{\mathbf{e}}_\theta \otimes \underline{\mathbf{e}}_\theta\right) \tag{2}$$

$$\underline{\underline{\mathbf{D}}} = D_{33}\left(\underline{\mathbf{e}}_3 \otimes \underline{\mathbf{e}}_3 - \frac{1}{2}\underline{\mathbf{e}}_r \otimes \underline{\mathbf{e}}_r - \frac{1}{2}\underline{\mathbf{e}}_\theta \otimes \underline{\mathbf{e}}_\theta\right) \tag{3}$$

Influence of the initial diameter on stress levels

Figure 4 represents the evolution of the mean axial stress $\bar{\sigma}_{33}$ as a function of the axial logarithmic strain ε_{33} when $D_{33} = 10^{-1}$ s^{-1} for $f = 20\%$ and C_1. The two plotted curves have been obtained with two different

[1]For the rest of the document, compressive axial strains and stresses will be plotted as positive data.

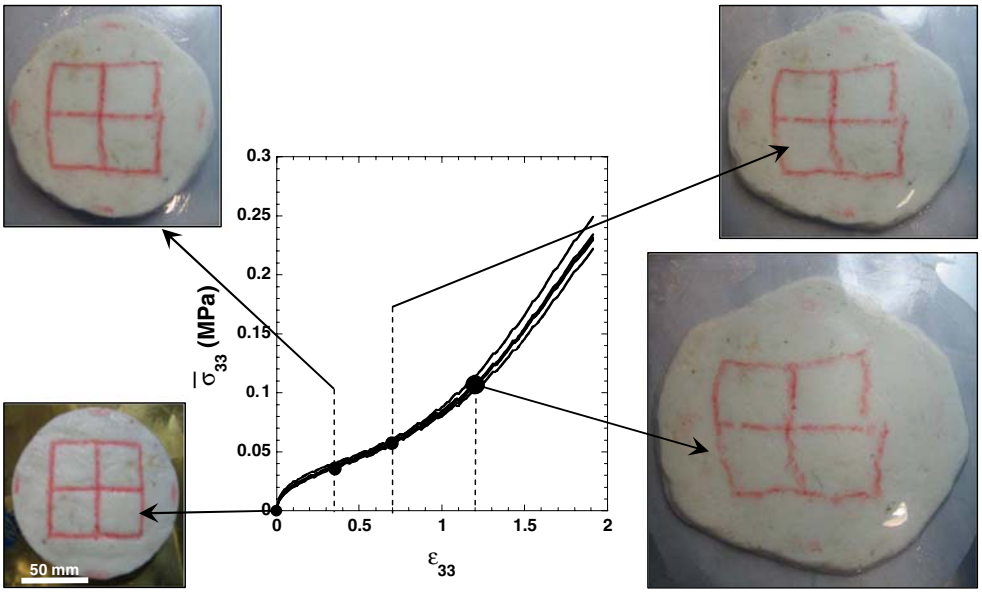

Fig. 3 General aspects of a sample at different strains and typical stress–strain curves recorded for five different samples (C_1, $f = 20\%$, $D_{33} = 0.1\ s^{-1}$)

initial diameters $2R_0$, i.e. 70 and 110 mm. Firstly, as shown from this figure, the scattering of the results given by the error bars is higher for the small-diameter samples (±25%) than for the larger ones (±10%). This can partially be ascribed to the experimental procedure used to process samples. Secondly, the figure clearly reveals that stress levels are higher for samples with the larger diameter. This may be induced by the shearing of the lubricating layer during the flow. In the next subsection, a proposition is made to get rid of such artefacts.

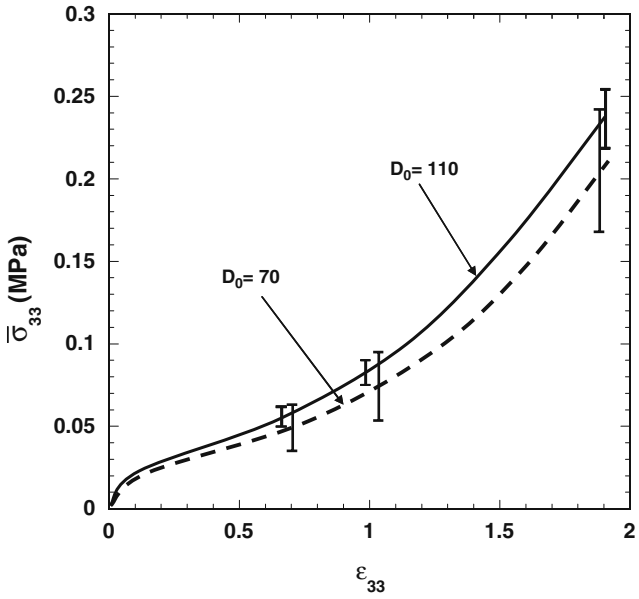

Fig. 4 Influence of the diameter of samples (in mm) on stress-strain measurements (C_1, $f = 20\%$, $D_{33} = 0.1\ s^{-1}$)

Correction of compression curves

To account for possible axial stresses induced by the lubricating layer, a plug flow model is proposed (see Fig. 5). It is very similar to plug flow models developed to model flow of SMC or GMT during compression mouldings (Barone and Caulk 1986; Abrams and Castro 2003; Dumont et al. 2007a). For that purpose, BMCs are supposed to be incompressible one-phase continua exhibiting transverse isotropy of axis $\underline{\mathbf{e}}_3$. It is supposed that the strain rate state is homogeneous in deformed samples (following Eq. 3), although the lubricant exerts shear stresses on their upper and lower surfaces. Hence, the velocity $\underline{\mathbf{v}}$ of a material point in a given BMC sample is written as:

$$\underline{\mathbf{v}} = \frac{\dot{h}}{h}\left(x_3\underline{\mathbf{e}}_3 - \frac{1}{2}r\underline{\mathbf{e}}_r\right), \tag{4}$$

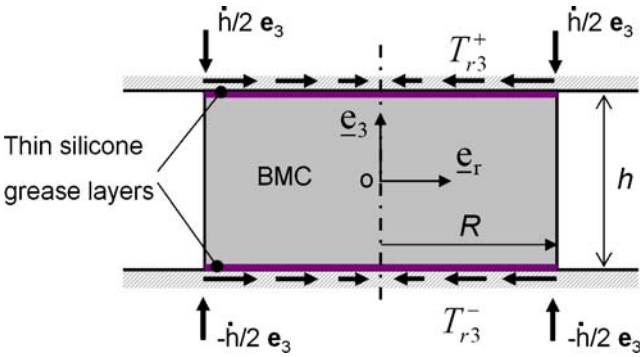

Fig. 5 Schematic representation of the plug flow assumptions used to account for the influence of the silicone grease during tests

x_3 being the altitude of the considered point from the midplane of the cylindrical sample and r being its radius. In accordance with the above kinematical and mechanical assumptions, the BMC stress tensor can be written as:

$$\underline{\underline{\boldsymbol{\sigma}}} = -p\underline{\underline{\boldsymbol{\delta}}} + T_{r3}\left(\underline{\mathbf{e}}_r \otimes \underline{\mathbf{e}}_3 + \underline{\mathbf{e}}_3 \otimes \underline{\mathbf{e}}_r\right) + \underline{\underline{\boldsymbol{\sigma}}}^e, \tag{5}$$

where p is the incompressibility pressure, $\underline{\underline{\boldsymbol{\delta}}}$ the identity tensor and $\underline{\underline{\boldsymbol{\sigma}}}^e$ the extra stress tensor. The shear stress T_{r3} is a Lagrange multiplier which is added to constrain the shear strain rate D_{r3} to zero inside the sample (see Eq. 3). For the sake of simplicity, shear stresses T_{r3}^+ and T_{r3}^- that the lubricating layers exert, respectively, on the upper ($x_3 = h/2$) and lower ($x_3 = -h/2$) surfaces of the sample are supposed to be written as (see Fig. 5):

$$T_{r3}^+ = T_{r3}^- = \lambda\frac{\dot{h}}{2h}r, \tag{6}$$

where λ is a positive constant hydrodynamic friction coefficient. Notice that more complex hydrodynamic or Coulombic friction coefficient can be introduced (Barone and Caulk 1986; Abrams and Castro 2003; Dumont et al. 2007a).

Therewith, the momentum balance equations of the BMC are written and integrated along the thickness h of the BMC, assuming quasi-static evolutions. In particular, along $\underline{\mathbf{e}}_r$ and $\underline{\mathbf{e}}_\theta$, one obtains:

$$\begin{cases} -P_{,r} + \dfrac{1}{h}\left(T_{r3}^+ + T_{r3}^-\right) = 0 \\ -P_{,\theta} = 0 \end{cases} \text{ where } P = \frac{1}{h}\int_{-h/2}^{h/2} p\,dx_3. \tag{7}$$

Together with the zero stress boundary condition on the lateral free surface of the sample (located at $r = R = R_0\sqrt{h_0/h}$), the last system yields:

$$P(r) = \sigma_{rr}^e + \lambda\frac{\dot{h}}{4h^2}\left(r^2 - R_0^2\frac{h_0}{h}\right). \tag{8}$$

It is also possible to calculate the mean axial stress $\bar{\sigma}_{33}$:

$$\bar{\sigma}_{33} = \frac{F_3}{\pi R^2} = -\frac{2}{R^2}\int_0^R p(r, x_3)rdr + \sigma_{33}^e,\ \forall\, x_3. \tag{9}$$

The mean axial stress writes in particular for $x_3 = h/2$:

$$\bar{\sigma}_{33} = -\frac{2}{R^2}\int_0^R p(r, h/2)rdr + \sigma_{33}^e. \tag{10}$$

Moreover, the global form of momentum balance equation along $\underline{\mathbf{e}}_3$ allows us to write:

$$\int_0^R p(r, x_3)rdr = \int_0^R p(r, h/2)rdr, \tag{11}$$

so that it can be easily shown that (Dumont et al. 2007a)

$$\int_0^R P(r)rdr = \int_0^R p(r, h/2)rdr. \tag{12}$$

Accounting for Eq. 8, the last expression allows us to obtain the following expression of $\bar{\sigma}_{33}$:

$$\bar{\sigma}_{33} = \sigma_{33}^e - \sigma_{rr}^e + \frac{\lambda}{8}\frac{\dot{h}}{h^2}R^2. \tag{13}$$

By noting that, under pure simple compression $\sigma_{33} = \sigma_{33}^e - \sigma_{rr}^e$, the corrected axial stress reads:

$$\sigma_{33} = \bar{\sigma}_{33} - \frac{\lambda}{8}\frac{\dot{h}}{h^3}h_0R_0^2, \tag{14}$$

It corresponds to the average axial stress from which the friction contribution has been subtracted. It is important to notice that, at this stage, such a correction requires a limited set of assumptions on the constitutive behaviour of the BMC (incompressibility + transverse isotropy).

The friction coefficient λ involved in Eq. 14 can be estimated by analysing tests performed with samples exhibiting two different initial diameters. As shown by the examples given in Fig. 6, Eq. 14 allows fairly good corrections of stress–strain curves. Hence, λ was estimated to $2\ 10^{-4}$, 10^{-3} and $2\ 10^{-3}$ N s mm^{-3} for fibre contents of 0%, 10% and 20%, respectively. Various reasons could explain this trend: reduction of the amount of remaining grease layers as the fibre content increases, tribological effects induced by the interaction between fibres and the compression plateaux, etc.

Results

Influence of the imposed strain and strain rate

Figure 7a contains a set of representative results showing the evolution of the axial stress σ_{33} with respect to the axial strain ε_{33} for three different constant axial

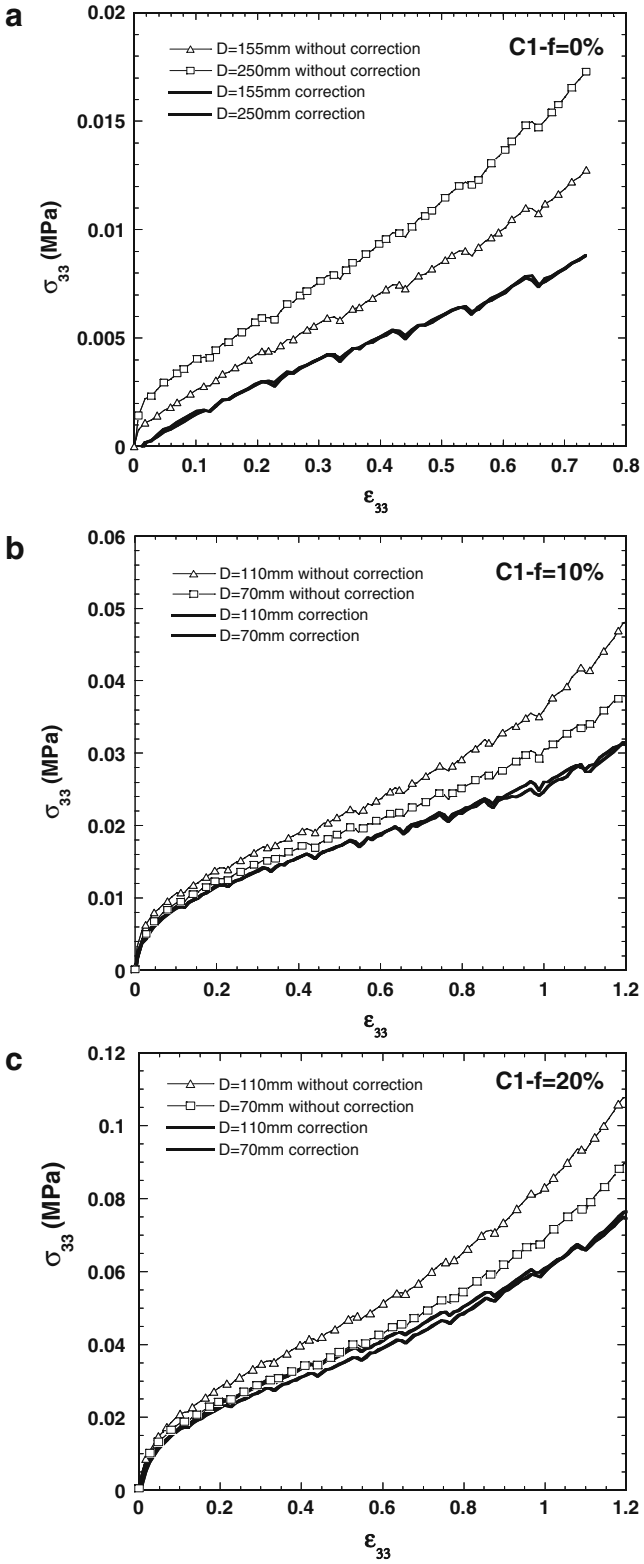

Fig. 6 Correction of the stress–strain curves to account for lubrication stresses for various fibre contents **a** 0%, **b** 10% and **c** 20% (C_1, $D_{33} = 0.1\ s^{-1}$)

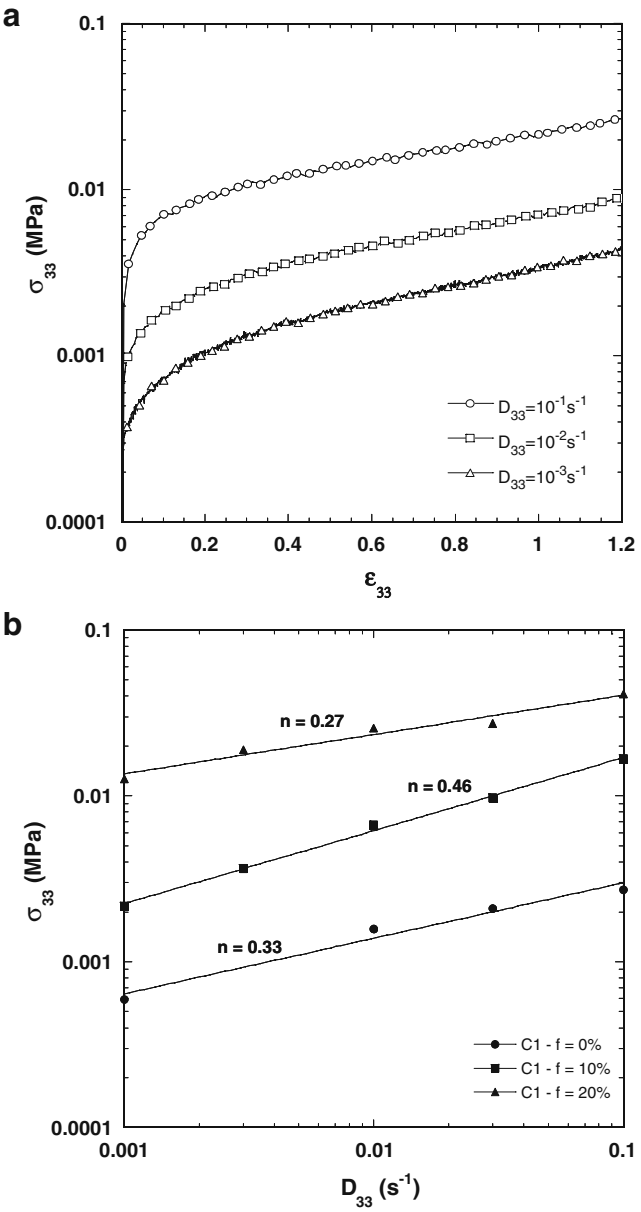

Fig. 7 **a** Stress–strain curves showing the influence of the axial strain rate D_{33} on the axial stress σ_{33} (C_1, $f = 10\%$). **b** Evolution of σ_{33} at a given axial strain $\varepsilon_{33} = 0.7$ as a function of D_{33}, for different contents of fibres (C_1). *Straight lines* represent power laws used to fit the experimental data (*marks*)

strain rates D_{33} and for $f = 10\%$. It clearly appears that the axial stress σ_{33} increases with both the axial strain ε_{33} and the axial strain rate D_{33}. The figure proves that BMCs exhibit strain hardening and pronounced viscous behaviour. To better illustrate this, the evolution of the axial stress σ_{33} with the axial strain rate D_{33} for a given axial strain ε_{33} chosen equal to 0.7 is reported in

Fig. 7b for all tested fibre fractions. Symbols represent the experimental points, whereas the lines represent power-laws used to fit experimental data:

$$\sigma_{33} = \eta_s(\varepsilon_{33},\, f) D_{33}^{n(\varepsilon_{33},\, f)}, \tag{15}$$

where η_s is the consistency and n the strain rate sensitivity. Both parameters are functions of the imposed axial strain ε_{33} and the fibre fraction f. Their evolution is given, respectively, in Fig. 8a, b as a function of the strain ε_{33} for all tested fibre fractions $f = 0\%, 10\%$ and 20%. One has to notice the pronounced shear thinning behaviour of BMC materials as $0.1 < n < 0.6$ and the significant decrease of this parameter with increasing ε_{33}. On the contrary, the consistency increases with ε_{33}.

Influence of the strain rate loading path

The influence of the strain rate loading path on the BMC rheology is depicted in Fig. 9a, where the evolution of σ_{33} with ε_{33} is depicted in cases where the strain rate D_{33} is increased (resp. decreased) from 10^{-3} to 10^{-1} s^{-1} (resp. 10^{-1} to 10^{-3} s^{-1}), as well as in cases of constant strain rates loading path. As shown in these figures, when a transition occurs between two imposed

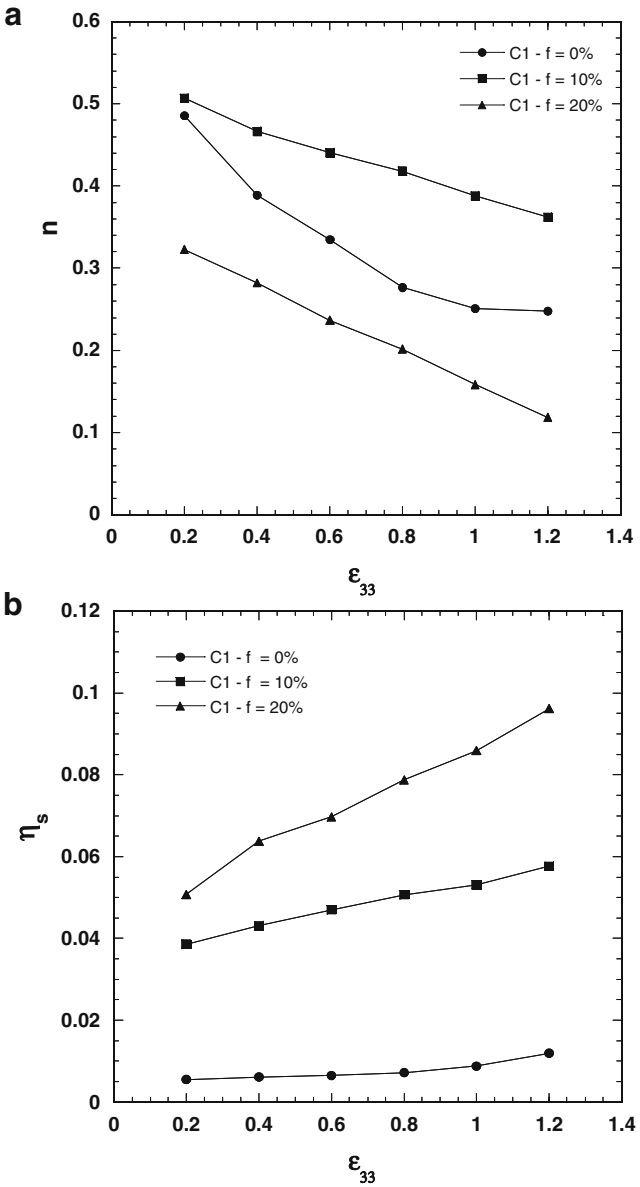

Fig. 8 Evolution of the power-law exponent n (**a**) and the consistency η_s (**b**) of the fitted power laws as a function of the considered axial strain ε_{33} and for various fibre content (C_1)

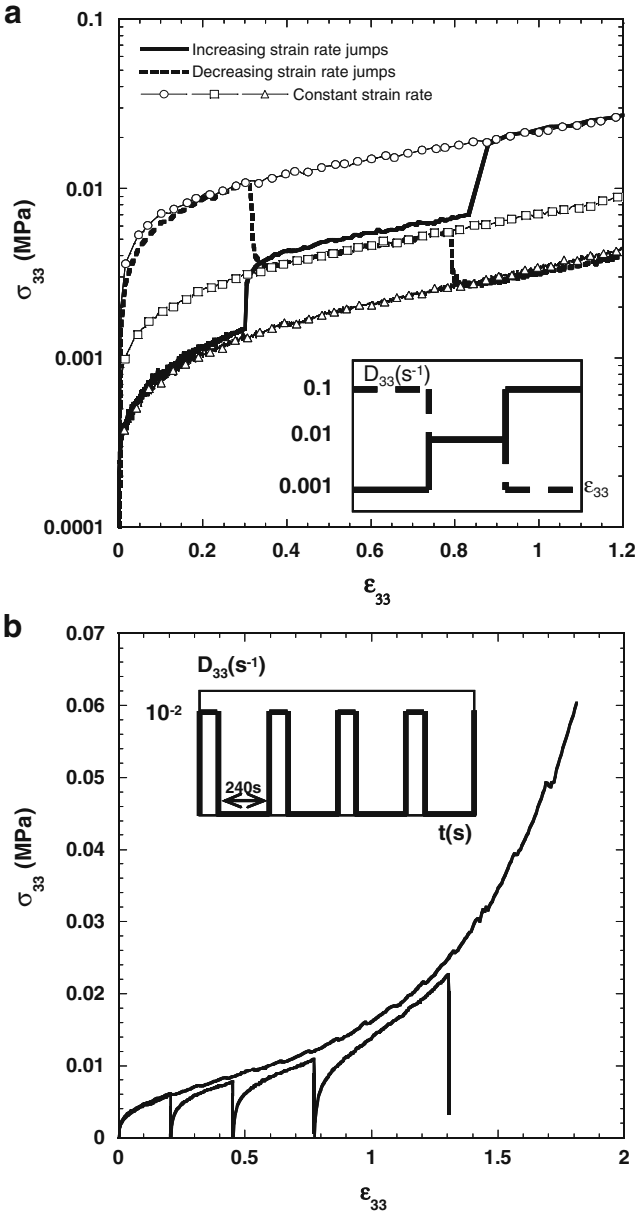

Fig. 9 Influence of the strain rate loading path on stress–strain curves (C_1, $f = 10\%$)

values of D_{33}, curves exhibit rather short transient regimes and reach quite rapidly curves obtained at constant strain rates. Similar observations are made when crenellated profiles are imposed for D_{33}, as it can be observed in Fig. 9b. Moreover, in this case, one can notice that, during the 240-s relaxations, stress levels fall down to zero, except for the last relaxation, for which a small residual stress is recorded.

Influence of the mass fraction of fibres

Figure 10 collects three stress–strain curves obtained when deforming at $D_{33} = 10^{-1}$ s^{-1} BMC samples having three different fibre mass fractions. A tremendous increase of stress levels is recorded with the fibre content. For instance, at a strain $\varepsilon_{33} = 1.2$, the axial stress measured for BMCs with $f = 20\%$ is 35 times higher than for BMCs without fibres. This can be correlated to the observed increases of the consistency previously described in Fig. 7b. Please note that similar tendencies were previously observed for quite similar materials, such as SMC (Dumont et al. 2003) or model transparent fibre-bundle suspensions (Dumont et al. 2007b).

Influence of the polydispersity of the fillers

The influence of the types of fillers C_1 and C_2 on stress–strain curves was investigated in cases of BMCs without fibres (Fig. 11a) and with a fibre content $f = 20\%$ (Fig. 11b). As expected (Coussot 1999), Fig. 11a shows that stress levels are lower for the wider particle distributions, i.e. for C_1. Here, it is important to notice that this trend remains preserved when a significant amount of fibres is added to BMCs and stress levels are considerably increased, as can be observed in Fig. 11b.

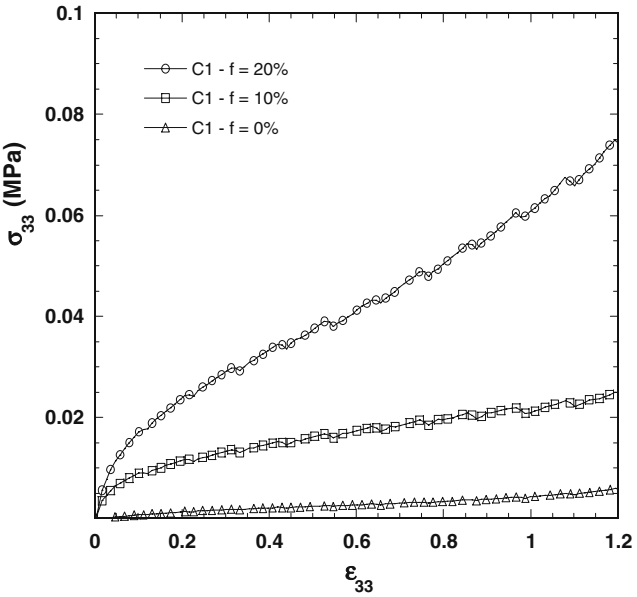

Fig. 10 Influence of the fibre content on stress–strain curves (C_1, $D_{33} = 0.1$ s^{-1})

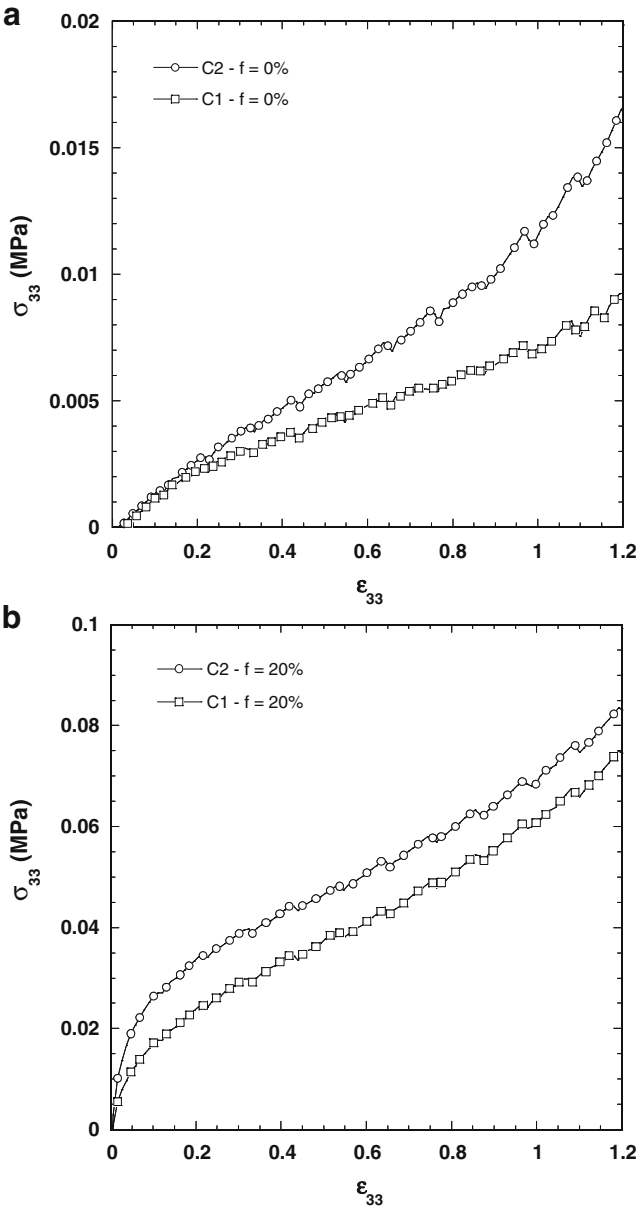

Fig. 11 Influence of the polydispersity of the Al_2O_3 filler on stress–strain curves ($D_{33} = 0.1$ s^{-1}): without fibres, $f = 0\%$ (**a**), with fibres, $f = 20\%$ (**b**)

Discussion

Experimental results that have been obtained in this work bring up the following comments, valid for the

two types of mineral fillers and within the investigated fibre content, strain rate and strain ranges:

- Whatever the fibre content, types of mineral fillers and strain and strain rates, the considered concentrated suspensions exhibit a pronounced and dominant viscous behaviour. Consequently, following the classification proposed by Coussot and Ancey (1999), this suggests that local deformation mechanisms, i.e. relative motions between solid particles (Al_2O_3 particles + glass fibres), are mainly ruled by viscous lubrication forces induced by polymers used in the paste formulation.
- The compression viscosity $\eta_{33} = \sigma_{33}/D_{33}$ is non-Newtonian; it is a power-law function of the axial strain rates within the investigated strain rate range. The power-law exponent n decreases with the imposed strain, whereas the consistency η_s increases. Such a non-Newtonian behaviour may be ascribed to the configurations of mineral particles and fibres (spatial distributions of mineral particles and glass fibres + orientation of fibres), which evolve with the imposed strain rates and strains.
- Some elastic effects have also been observed during strain rate jumps. This may be correlated with the elasticity of the polymers contained in the matrix, but also to the elasticity of the fibres that may be subjected to possible bending during flow.

From these experimental observations, a very simple 1D and non-linear macroscopic viscoelastic model is proposed to reproduce phenomenologically experimental trends. It is clear that more sophisticated rheological models that would account, by using well-chosen internal variables, for the evolution of particles' distribution and orientation would be much more appropriate. However, to build them and identify their constitutive parameters, further dedicated experiments and a deeper analysis of the evolving microstructures of the suspensions would be required. The preliminary experiments presented here are not sufficient to reach this goal. Thus, the total strain rate D_{33} (resp. the strain ε_{33}) is split into two contributions, i.e. an elastic one D^e_{33} (resp. ε^e_{33}) and a purely viscous one D^v_{33} (resp. ε^v_{33}):

$$D_{33} = D^e_{33} + D^v_{33}, \quad \varepsilon_{33} = \varepsilon^e_{33} + \varepsilon^v_{33}. \tag{16}$$

The viscous strain rate D^v_{33} is linked with the total axial stress σ_{33} by the following constitutive equation:

$$\sigma_{33} = \eta_p \left(1 + \alpha f^2\right) \left(D^v_{33}\right)^n \mathrm{e}^{k\varepsilon^v_{33}}. \tag{17}$$

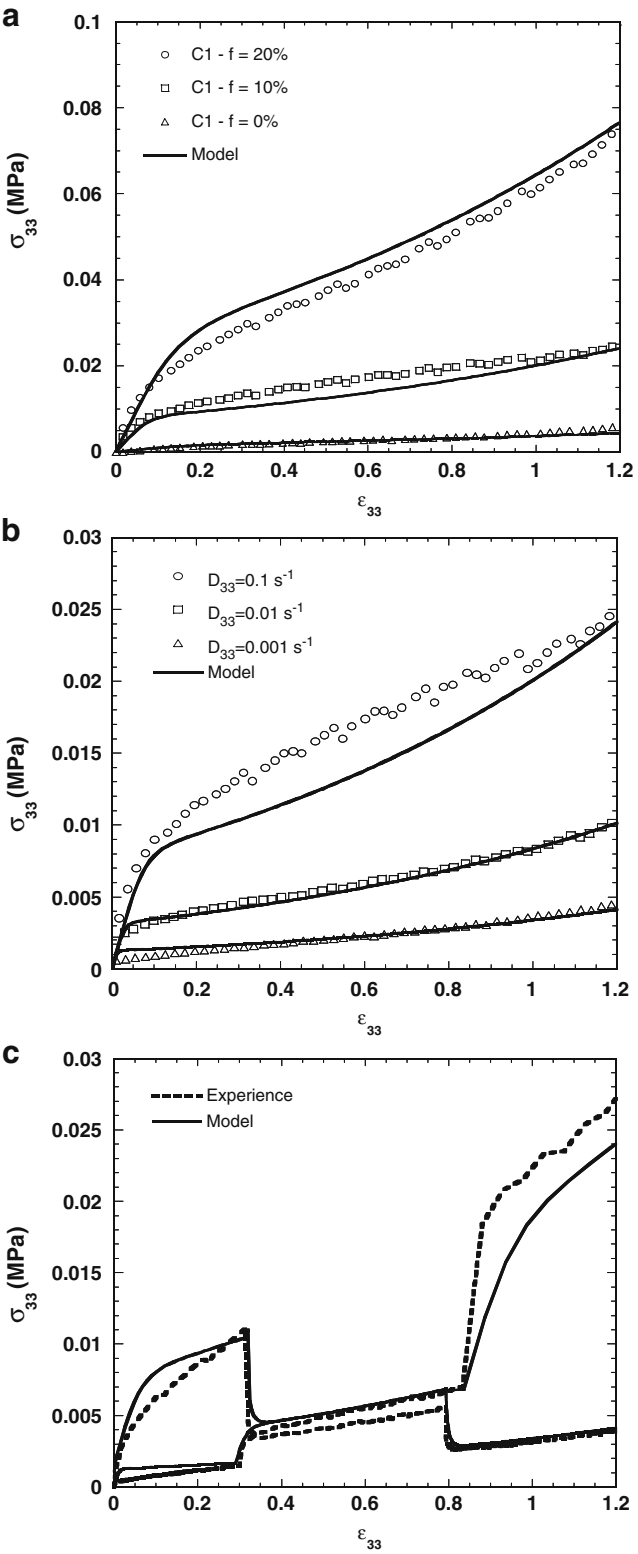

Fig. 12 Comparison between model predictions and experimental results (C_1), at various fibre contents ($D_{33} = 0.1s^{-1}$) (**a**) and at various constant (**b**) or variable (**c**) axial strain rates ($f = 10\%$)

In the above equation, η_p is closely linked with the consistency of the paste without fibre at low strains. The observed strain hardening is accounted by the exponential function involving the coefficient k. Based on results obtained with rather close polymer composites (Dumont et al. 2003, 2007b), a quadratic evolution of stress levels is assumed, involving the coefficient α. The elastic strain ε^e_{33} is linked with σ_{33} by the following relation:

$$\sigma_{33} = E_p(1+\beta f)\varepsilon^e_{33}, \tag{18}$$

where E_p is the elastic modulus of the paste without fibre and β is a constant. Hence, the incremental form of the model reads:

$$D_{33} = \frac{\dot{\sigma}_{33}}{E_p(1+\beta f)} + \left(\frac{\sigma_{33}}{\eta_p(1+\alpha f^2)\mathrm{e}^{k\varepsilon^v_{33}}}\right)^{\frac{1}{n}} \tag{19}$$

Constitutive parameters η_p, α, n, k, E_p and β, involved in the above equations, have been fitted on experimental results. They are, respectively, equal to 0.004 MPa s, 400, 0.4, 1, 0.01 MPa and 100. As shown in Fig. 12, the model permits a rather good description of experimental trends.

Conclusion

BMCs can be seen as granular suspensions of mineral fillers embedded in a polymer matrix, which is reinforced with glass fibres. Their rheology was here studied by performing a preliminary set of lubricated compression experiments. The following points summarise the main experimental results:

- To account for friction effects due to the thin layers of silicone grease sheared between the compression plateaux and the samples, a correction of recorded stress levels was proposed, requiring few assumptions concerning the BMC's rheological behaviour.
- The last one exhibits a pronounced viscous behaviour: it is mainly ruled by viscous lubrication efforts arising at the local scale between touching or almost touching particles (mineral fillers and glass fibres).
- Adding fibres to the pasty matrix significantly increases the viscosity of BMCs.
- A wider distribution of the Al_2O_3 particles' size tends to diminish the viscosity of BMC without fibres. This trend is still preserved when adding 20% glass fibres within the paste.
- The evolution of the spatial distribution and orientation of these particles induce a complex non-Newtonian behaviour. To better understand it, further experiments combined with microstructure observations are needed.

Lastly, to build 3D rheological models that could be implemented in injection moulding softwares, BMC samples should be subjected to other types of mechanical loadings, such as plane strain compression and simple shear. This work is planned.

Acknowledgements The authors would like to thank Compositec (Y. Gardet) for supplying BMC materials, as well as Schneider Electric (C. Venet) and the Fédération Rhône-Alpes Matériaux de Structures (FedeRAMS) for their financial support.

References

Abrams L, Castro J (2003) Predicting molding forces during sheet molding compound (SMC) compression molding. I: model development. Polym Compos 24:291–303

Barone MR, Caulk DA (1986) A model for the flow of a chopped fiber reinforced polymer compound in compression molding. J Appl Mech 53(191):361–370

Blanc R, Agassant JF, Vincent M (1992) Injection molding of unsaturated polyester compounds. Polym Eng Sci 32(19): 1440–1450

Boyard N, Millischer A, Sobotka V, Bailleul J-L, Delaunay D (2007) Behaviour of a moulded composite part: modelling of dilatometric curve (constant pressure) or pressure (constant volume) with temperature and conversion degree gradients. Compos Sci Technol 67:943–954

Coussot P (1999) Rhéophysique des pâtes et des suspensions. EDP Science, Les Ulis

Coussot P, Ancey C (1999) Rheophysical classification of concentrated suspensions. Phys Rev E 59:4445–4457

Deslandes N, Bellenger V, Jaffiol F, Verdu J (1998) Relationship between morphology and solvent interactions of a polyester composite material. Compos Part A Appl Sci Manuf 29:1481–1487

Dumont P, Orgéas L, Favier D, Pizette P, Venet C (2007a) Compression moulding of SMC: in situ experiments, modelling and simulation. Compos Part A Appl Sci Manuf 38: 353–368

Dumont P, Orgéas L, Le Corre S, Favier D (2003) Anisotropic viscous behaviour of sheet molding compounds (SMC) during compression molding. Int J Plast 19(4):625–646

Dumont P, Vassal J-P, Orgéas L, Michaud V, Favier D, Månson J-E (2007b) Processing, characterization and rheology of transparent concentrated fibre bundle suspensions. Rheol Acta 46:639–641

Estellé P, Lanos C, Perrot A, Servais C (2006) Slipping zone location in squeeze flow. Rheol Acta 45:444–448

Kenny J, Opalicki M (1996) Processing of short fibre/thermosetting matrix composites. Compos Part A Appl Sci Manuf 27A(3):229–240

Lafranche E, Menio S, Guegan M-L, Krawczak P (2002) Étude expérimentale des mécanismes d'écoulement dans

le moulage par injection des BMC. Rev Compos Mater Av 12:461–475

Le TH, Dumont PJJ, Orgéas L, Favier D, Salvo L, Boller E (2008) X-ray phase contrast microtomography for the analysis of the fibrous microstructure of SMC composites. Compos Part A Appl Sci Manuf 39:91–103

Le Corre S, Orgéas L, Favier D, Tourabi A, Maazouz A, Venet C (2002) Shear and compression behaviour of sheet molding compounds. Compos Sci Technol 62(4):571–577

Ma C-CM, Hsieh C-T, Kuan H-C, Tsai T-Y, Yu S-W (2003) Effects of molecular weight and molecular structure of low profile additives on the properties of bulk molding compounds (BMC). Polym Eng Sci 43(5):989– 998

Millischer A, Delaunay D (2001) Experimental and numerical analysis of heat transfer in bulk molding compound injection process. J Reinf Plast Compos 20: 495–512

Vallat M-F, Schultz J, Mauzac C, Jacquin M (1999) Characterization of the surface of bulk-molded compounds. Polym Adv Technol 10:237–243

Vayer M, Serré C, Boyard N, Sinturel C, Erre R (2002) Surface morphologies of composites based on saturated polyester pre-polymer. J Mater Sci 37:2043–2051